The Astronomical Journal, 153:205 (7pp), 2017 May https://doi.org/10.3847/1538-3881/aa65d1

The Oblique Orbit of WASP-107b from *K2* Photometry

Fei Dai[1,2] and Joshua N. Winn[2]

[1] Department of Physics and Kavli Institute for Astrophysics and Space Research, Massachusetts Institute of Technology, Cambridge, MA 02139, USA; fd284@mit.edu

[2] Department of Astrophysical Sciences, Peyton Hall, 4 Ivy Lane, Princeton, NJ 08544, USA

Received 2017 February 9; revised 2017 March 6; accepted 2017 March 7; published 2017 April 7

Abstract

Observations of nine transits of WASP-107 during the *K2* mission reveal three separate occasions when the planet crossed in front of a starspot. The data confirm the stellar rotation period to be 17 days—approximately three times the planet's orbital period—and suggest that large spots persist for at least one full rotation. If the star had a low obliquity, at least two additional spot crossings should have been observed. They were not observed, giving evidence for a high obliquity. We use a simple geometric model to show that the obliquity is likely in the range 40°–140°, i.e., both spin–orbit alignment and anti-alignment can be ruled out. WASP-107 thereby joins the small collection of relatively low-mass stars with a high obliquity. Most such stars have been observed to have low obliquities; all of the exceptions, including WASP-107, involve planets with relatively wide orbits ("warm Jupiters," with $a_{\rm min}/R_\star \gtrsim 8$). This demonstrates a connection between stellar obliquity and planet properties, in contradiction to some theories for obliquity excitation.

Key words: planetary systems – planets and satellites: individual (WASP-107) – stars: individual (WASP-107)

Supporting material: data behind figure

1. Introduction

A star's obliquity is a fundamental geometric property of a planetary system, and an intriguing piece of the puzzle of planet formation and orbital evolution (as recently reviewed by Winn & Fabrycky 2015). Many methods have been devised to test for alignment between stellar rotation and planetary orbital motion: the Rossiter–McLaughlin effect (Queloz et al. 2000), gravity darkening (Barnes 2009; Masuda 2015), $v \sin i$ statistics (Schlaufman 2010), asteroseismology (Chaplin et al. 2013), and the spot-tracking method (Nutzman et al. 2011; Sanchis-Ojeda et al. 2011; Mazeh et al. 2015a). One of these methods, the spot-tracking method, takes advantage of precise and continuous time-series photometry of stars with transiting planets, which the *Kepler* mission has provided (Borucki et al. 2011). When a transiting planet crosses in front of a starspot, the loss of light is briefly reduced, because the hidden portion of the star has a lower intensity than the surrounding photosphere. The detection and timing of these events can sometimes reveal the stellar obliquity. One approach is to seek evidence for multiple crossings of the same spot, which are more likely to occur for a spin-aligned star than a tilted star (see, e.g., Désert et al. 2011; Nutzman et al. 2011; Sanchis-Ojeda et al. 2011).

WASP-107b is a transiting planet discovered by Anderson et al. (2017). The host star is a K dwarf of mass 0.69 $M_\star$. The planet has an orbital period of 5.7 days and a radius of 0.95 $R_{\rm Jup}$. Despite this near-Jovian size, radial-velocity monitoring revealed the planet's mass to be only about twice that of Neptune's (0.12 $M_{\rm Jup}$). This makes the planet difficult to classify and demonstrates that such a relatively low mass is sufficient to accrete a large gaseous envelope.

WASP-107 happened to be within the field of view of *K2* Campaign 10, which is one of the star fields along the ecliptic that are being monitored by the *Kepler* telescope (Howell et al. 2014). Thanks to a proposal by Anderson et al. (2017), WASP-107 was observed with one-minute sampling ("short cadence"). In this paper, we report on our analysis of the *K2* photometry and our assessment of the stellar obliquity, based on observations of starspot crossings. The following section describes the data reduction. In Section 3, we refine the basic transit parameters and identify spot crossings. Section 4 is concerned with the stellar rotation period, a crucial ingredient in the analysis of starspot crossings. In Section 5, we present evidence for a high obliquity by modeling the intersections between the planet's transit chord and the possible paths of starspots. We discuss the implications in Section 6.

2. *K2* Photometry

WASP-107 (or EPIC 228724232) was observed by *Kepler* from 2016 July 6 to September 20 in the short-cadence mode. We disregarded the first 6 days of data, which were of lower quality because of a 3.5 pixel pointing error that was subsequently corrected. A further complication was the loss of Module 4 during this campaign, resulting in a 14-day gap in data collection. Thus, the useful data comprises an interval of about 7 days, followed by the 14-day gap, and then a continuous interval of nearly 50 days.

We downloaded the pixel files from the Mikulski Archive for Space Telescopes.[3] To reduce the spurious intensity fluctuations caused by the rolling motion of the spacecraft, we used an approach similar to that described by Vanderburg & Johnson (2014). We considered a circular aperture of radius 4.5 pixels centered on the brightest pixel and fitted a two-dimensional Gaussian function to the intensity distribution within the aperture. Then, we decorrelated the aperture-summed flux and the X and Y positions of the fitted Gaussian function. Figure 1 shows the corrected time series, including stellar variability, transit signals, and some residual systematic effects.

[3] https://archive.stsci.edu/k2

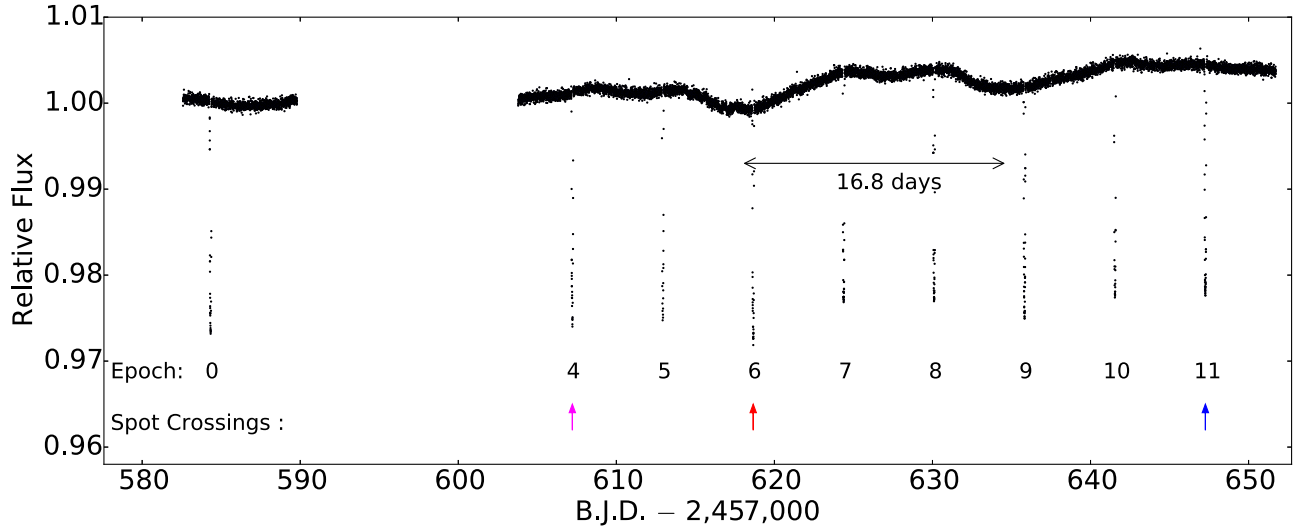

Figure 1. Corrected *K2* photometry of WASP-107. Colored arrows indicate the transits during which spot-crossing anomalies were detected. Outside of transits, the time between the two clearest minima is 16.8 days, which agrees with the previously measured rotation period. The data used to create this figure are available.

3. Light Curve Analysis

Anderson et al. (2017) found the stellar rotation period to be nearly three times as long as the orbital period. If the stellar obliquity were near 0° or 180°, then the spots would move along the transit chord as the star rotates. In such a situation, whenever we see a spot-crossing anomaly during transit epoch n, we would also expect to see one in epochs $n-3$ or $n+3$, as long as the starspot persists for at least one rotation. We checked for this pattern by scrutinizing the data obtained during each of the 9 transits. A spot-crossing anomaly was obvious to the eye in epoch 4, but none were visible in epoch 7 (and epoch 1 occurred during the data gap). A second spot crossing took place in epoch 6, but none were detected in epochs 3 or 9. A third possible anomaly, weaker than the others, was seen in epoch 11, but none were seen in epoch 8. Thus, it was immediately clear that WASP-107 is unlikely to have a perfectly prograde or retrograde orbit. A tilt of order $R_p/R_\star$ radians ($\sim 10^\circ$) is needed for the spots to leave the transit chord as they rotate across the visible stellar hemisphere.

For quantitative analysis, we modeled each transit light curve with the `Batman` code written by Kreidberg (2015). We considered a 7 hr window around the time of mid-transit and allowed the out-of-transit flux to be a quadratic function of time in order to account for longer-term stellar variability. The free parameters included the planet-to-star radius ratio ($R_p/R_\star$), the ratio of stellar radius to orbital distance ($R_\star/a$), and the impact parameter ($b \equiv a\cos I/R_\star$). We took the limb-darkening profile to be quadratic, with both coefficients u_1 and u_2 as free parameters. We also took into account the effect of untransited starspots, which increase the transit depth beyond what it would be in the absence of spots. To do so, we introduced an additional parameter $\Delta F_{\rm spot}$ specific to each transit, such that

$$F_{\rm calc,spot} = \frac{F_{\rm calc,no\text{-}spot} - \Delta F_{\rm spot}}{1 - \Delta F_{\rm spot}}. \quad (1)$$

Here, $F_{\rm calc,no\text{-}spot}$ is the calculated flux using `Batman`, and $F_{\rm calc,spot}$ is the calculated flux that is compared to the observed flux. With this definition, $F_{\rm calc,spot} \equiv 1$ outside of the transits; this was needed because we normalized the data in this manner. We adopted the usual χ^2 likelihood function and found the maximum-likelihood solution using the Levenberg–Marquardt algorithm as implemented in the `Python` package `lmfit` (Newville et al. 2014).

To determine the number of spot-crossing events during each transit, we modeled the spot-crossing anomalies as Gaussian functions of time:

$$F_{\rm anom}(t) = A\exp\left[-\frac{(t-t_{\rm anom})^2}{2\sigma_{\rm anom}^2}\right] \quad (2)$$

where A, $t_{\rm anom}$, and $\sigma_{\rm anom}$ represent, respectively, the amplitude, time, and duration of the anomaly. To identify anomalies more objectively, we fitted each transit several times: with no anomalies, one anomaly, two anomalies, and so forth. Then we used the Bayesian Information Criterion,

$$\mathrm{BIC} = 2\log(L_{\rm max}) + N\log(M), \quad (3)$$

to decide which number of anomalies provides the best fit to the data. In this equation, $L_{\rm max}$ is the maximum likelihood, N is the number of model parameters, and M is the number of data points. We demanded $\Delta\mathrm{BIC} > 10$. Only three anomalies passed this criterion: the same three that were visually obvious. Table 1 reports their properties based on the Markov Chain Monte Carlo (MCMC) code of Foreman-Mackey et al. (2013). The quoted value is based on the 50% level of the cumulative posterior distribution, and the uncertainty interval is based on the 16% and 84% levels.

To refine the transit parameters, we excluded data within $2\sigma_{\rm anom}$ of the fitted time of each anomaly. Then, we produced a phase-folded anomaly free light curve, which was subjected to another MCMC analysis. Table 2 reports the results. Finally, to model the effects of the identified spot-crossing anomalies in detail, we switched from the phenomenological model of Equation (2) to the more physically motivated model `spot-rod` (Béky et al. 2014). In this model, the transit light curve is calculated for a limb-darkened photosphere with uniform and circular spots.

Table 1
Spot-crossing Anomalies Observed in *K2*

Epoch	$t_{\rm anom}$ (BJD − 2,454,833)	Amplitude A	Duration $\sigma_{\rm anom}$ (days)	Spot #
4	2774.20512 ± 0.00022	0.00298 ± 0.00012	0.00493 ± 0.00022	1
6	2785.64242 ± 0.00044	0.00156 ± 0.00012	0.00493 ± 0.00041	2
11	2814.26773 ± 0.00096	0.00064 ± 0.00017	0.0031 ± 0.0010	3

4. Stellar Rotation Period

Knowledge of the stellar rotation period is important for the analysis of spot crossings. The *K2* time series (Figure 1) shows variability at the 0.3% level on a timescale of ∼10 days, with what appear to be two cycles of a quasiperiodic function. These variations are characteristic of starspots being carried around by stellar rotation. One estimate of the rotation period is the interval between the two clearest minima, which we found to be 16.8 ± 1.2 days by fitting quadratic functions to the data surrounding each minimum. Another measure comes from the periodogram (Lomb 1976; Scargle 1982). After masking out the transits, the periodogram of the time series has a peak at $17.7^{+8.8}_{-2.8}$ days. Likewise, the autocorrelation method (McQuillan et al. 2013) gives an estimate of $17.0^{+2.1}_{-1.6}$ days. All of these estimates agree with (and are probably less accurate than) the period of 17.1 ± 1.0 days reported by Anderson et al. (2017) based on two seasons of WASP photometry. In what follows, we adopt $P_{\rm rot} = 17.1 \pm 1.0$ days.

The combination of $P_{\rm rot}$, $R_\star$, and $v \sin i_\star$ can be used to calculate the stellar inclination angle $i_\star$:

$$\sin i_\star = \frac{v \sin i_\star}{v} = \frac{v \sin i_\star}{2\pi R_\star / P_{\rm rot}}. \quad (4)$$

Anderson et al. (2017) reported $v \sin i_\star = 2.5 \pm 0.8$ km s^{-1} based on the observed broadening of the star's spectral lines. On the other hand, $v = 2\pi R_\star / P_{\rm rot} = 3.0 \pm 0.2$ km s^{-1} using the stellar radius in Table 2. The comparison provides only a very loose constraint on the orientation of the star: $\sin i_\star = 0.8 \pm 0.3$.

5. Spot-crossing Anomalies

At the time of an observed spot-crossing anomaly, the planet and the spot overlap on the sky. Given the rotation period and the star's orientation, we can calculate the spot's motion in the immediate future and past. For obliquities near 0°or 180°, the spot moves parallel to the transit chord and is likely to be crossed during the subsequent transits or to have been crossed in the previous transits. For higher obliquities, this is unlikely, because the spot's path only intersects the transit chord at one location. The underlying assumptions are that the spot lasts for at least one stellar rotation and that the spot is not much larger than the planet. These assumptions seem justified here, given the apparent coherence of the stellar variability over the ≈60-day observing interval and the small amplitude of the variations.

To determine the allowed range of obliquities for WASP-107, we used a Monte Carlo procedure. In each of 10^4 realizations, we drew values of $P_{\rm rot}$, $\cos i_\star$, and the sky-projected obliquity λ, from uniform distributions. We held the transit parameters fixed in this part of the analysis, because they are so precisely constrained. Given the rotation period and stellar orientation as well as the observed times of the 3 anomalies, we calculated the trajectories of each of the 3 spots over the entire time interval of the *K2* observations. Then, we computed a "badness of fit" statistic, by totaling up the number of data points for which an intersection between the planet and a spot was predicted but not observed.

Table 2
System Parameters of WASP-107

Parameter		References
Stellar Parameters		
$T_{\rm eff}$ (K)	4430 ± 120	A
log g (dex)	4.5 ± 0.1	A
[Fe/H] (dex)	+0.02 ± 0.10	A
$v \sin i_\star$ (km s^{-1})	2.5 ± 0.8	A
$M_\star$ ($M_\odot$)	0.69 ± 0.05	A
$R_\star$ ($R_\odot$)	0.66 ± 0.02	A
Apparent V mag	11.6	A
$P_{\rm rot}$ (days)	17.1 ± 1.0	A
u_1	0.6666 ± 0.0062	B
u_2	0.015 ± 0.011	B
Planetary Parameters		
P (days)	5.7214742 ± 0.0000043	B
T_c (BJD)	2457584.329897 ± 0.000032	B
$a/R_\star$	18.164 ± 0.037	B
a (au)	0.0558 ± 0.0018	B
R_p/R_*	0.14434 ± 0.00018	B
R_p ($R_{\rm Jup}$)	0.948 ± 0.030	B
M_p ($M_{\rm Jup}$)	0.12 ± 0.01	B
i (°)	89.8 ± 0.2	B
$b \equiv a \cos i / R_\star$	0.07 ± 0.07	B
e (assumed)	0	A

Note. A: Anderson et al. (2017); B: this work.

Figure 3 illustrates the geometry. The left panel shows the star at epoch 4 for the case $\lambda = 0°$ and $i_\star = 90°$. The starspot's location along the transit chord is fixed by the observed timing of the flux anomaly. The right panel shows the calculated location of the starspot at epoch 7. According to this model, a flux anomaly should have been observed about one-quarter of the way through the transit, but it was not. The dotted line shows all of the possible locations for the starspot when λ is allowed to vary. For high enough λ, the spot can avoid being crossed. Similar plots can be made for the anomalies observed in epochs 6 and 11.

The middle and right panels of Figure 2 illustrate the success of high-obliquity models and the failure of low-obliquity models. The data points are the residuals after subtracting the best-fitting transit model, allowing the spot-crossing anomalies to be seen more clearly. In the middle panel, a good fit is achieved by a model with true obliquity $\Psi = 45°$. Of course, many other high-obliquity models also fit the data. In the right panel, we show 20 spot models drawn randomly from our Monte Carlo procedure, all having $\Psi < 40°$. None of them

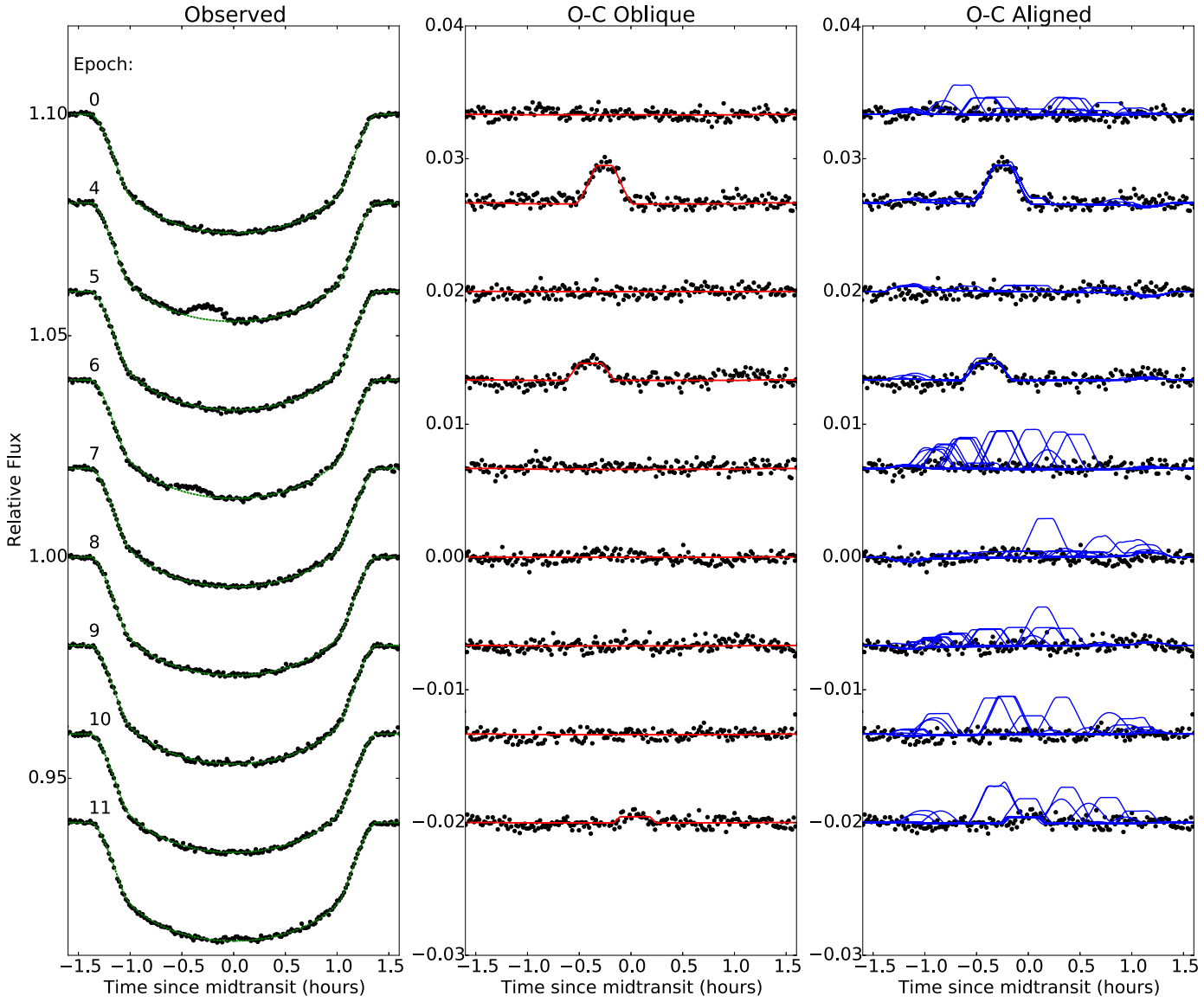

Figure 2. Transits of WASP-107. Left: all of the transits observed by *K2*. Epoch 1-3 are missing due to the loss of Module 4. Vertical offsets were applied to separate the individual transits. The dotted green line is the best-fitting model with no starspots. Middle: success of a high-obliquity model. Shown are residuals after subtracting the best-fitting no-spot model. The red curve is a representative model with obliquity $\Psi = 45°$ ($\lambda = 45°$, $i_\star = 90°$). Right: failure of low-obliquity models. The blue curves are 20 representative models with $\Psi < 40°$. By construction, these models fit the observed anomalies in Epochs 4, 6, and 11; however, they also predict additional spot-crossing events that are not observed.

provide a satisfactory fit, because they predict anomalies when none are seen.

Figure 4 summarizes the results. The left panel shows the badness-of-fit, as a function of $P_{\rm rot}$ and the true obliquity Ψ. Two horizontal lines indicate the 1σ range of the measured rotation period. All of the best fits are obtained for obliquities between 40° and 140°. Interestingly, there is a narrow range of rotation periods surrounding 17.16 days for which the obliquity must be restricted to a smaller interval to provide a good fit. This is because rotation periods in this range are nearly exactly three times longer than the orbital period. When this is the case, rotation brings the spot back to the transit chord just in time to intersect the planet, regardless of the stellar orientation. The right panel of Figure 4 shows the density (in parameter space) of all of the models that fit the data well and do not predict any unobserved anomalies. Here, we see more clearly that the successful models require the obliquity to be in the range from about 40° and 140°. Evidently, the star is tilted at some large angle, though we cannot specify the value of the angle with any precision.

6. Discussion

Should there be any doubt about our spot analysis, the high obliquity can be confirmed by detecting the Rossiter–McLaughlin (RM) effect during transits. The expected signal amplitude is

$$\Delta V_{\rm RM} \approx 0.7 (R_p/R_\star)^2 v \sin i_\star \approx 36 \,{\rm m\,s^{-1}}. \quad (5)$$

The situation brings to mind the case of HAT-P-11 (Bakos et al. 2010), in which the order of events was reversed. Winn et al. (2010b) found a high obliquity through RM spectroscopy,

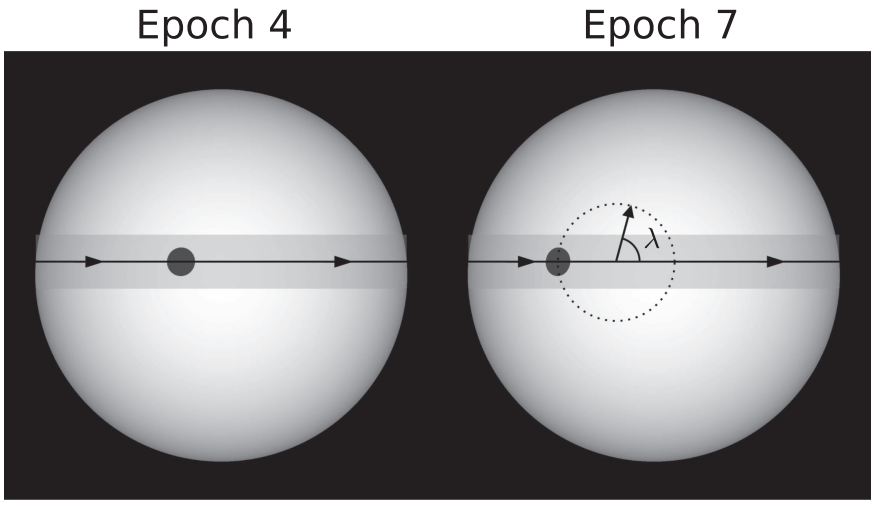

Figure 3. Illustration of the geometric model. Left: the star during Epoch 4, when a spot-crossing anomaly was observed just before mid-transit. The dark circle is the starspot and the gray bar is the path of the transiting planet. Right: the predicted situation in Epoch 7 for zero obliquity and $P_{\rm rot} = 18.1$ days. A spot-crossing anomaly should occur about one-quarter of the way through the transit, but is not observed. One way to avoid a spot crossing is to rotate the sky projection of the stellar rotation axis. By adjusting this angle λ, the predicted spot location can be changed to anywhere along the dotted line.

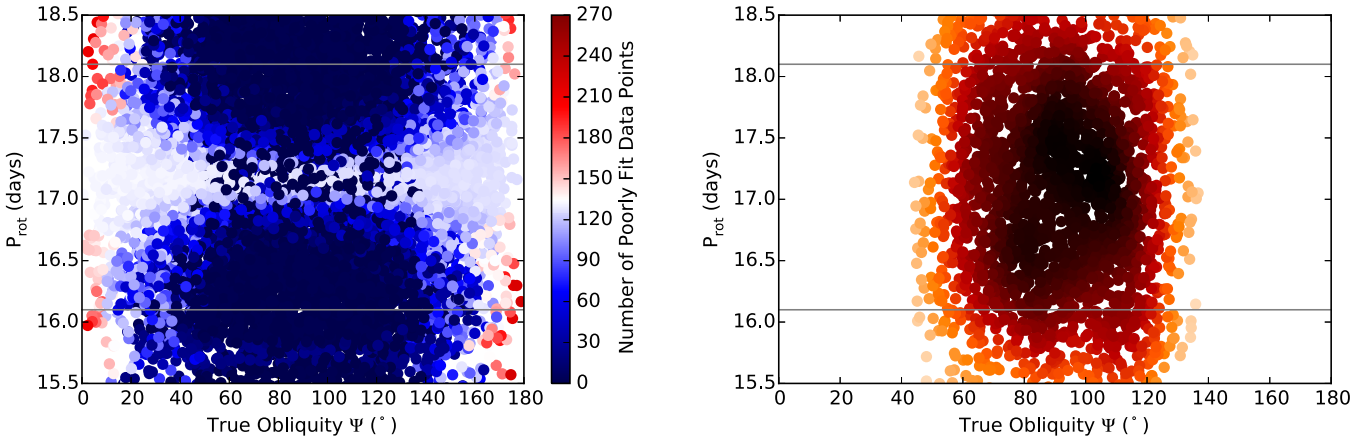

Figure 4. Monte Carlo search for stellar orientations consistent with the data. Left: the quality of fit as a function of obliquity and rotation period. Horizontal gray lines bound the 1σ range in the measured rotation period. The color encodes the number of data points where anomalies are predicted but not observed. Dark blue indicates a good fit, and dark red a poor fit, with white in between. Right: similar, but this time the color represents the density of good-fitting (no unobserved anomalies) models in parameter space. In these models, the true obliquity lies between about 40° and 140°.

but with a low signal-to-noise ratio; this finding was subsequently confirmed by spot modeling (Sanchis-Ojeda & Winn 2011; Deming et al. 2015). With an apparent magnitude $V = 11.6$, WASP-107 is about 2 mag fainter than HAT-P-11. This will make the RM observation more challenging, but probably not impossible given that the transit depth of WASP-107 is five times larger than that of HAT-P-11.

In fact, these two systems form an interesting pair for comparison. Both planets are "super-Neptunes" that orbit K dwarfs at similar orbital distances. For WASP-107 and HAT-P-11, respectively, the stellar masses are 0.69 and 0.80 $M_\odot$, the $a/R_\star$ values are 18.1 and 15.1, and the planet masses are 1.5 and 2.2 times the mass of Neptune. Additionally, both stars have high obliquities. The one prominent difference is that WASP-107b has a much larger diameter and is nine times less dense.

Both HAT-P-11 and WASP-107 are also exceptions to the general trend that relatively low-mass stars ($M \lesssim 1.2\,M_\odot$ or $T_{\rm eff} \lesssim 6200$ K) have low obliquities. Figure 5 gathers together all of the reliable obliquity measurements based on the RM effect, spot modeling, or asteroseismology.[4] The size of each data point encodes our confidence in each system's departure from perfect alignment; the largest points are almost certainly misaligned. The data are shown as a function of $M_p/M_\star$ and $a_{\rm min}/R_\star$, i.e., the pericenter distance $a(1-e)$ in units of the stellar radius. Red points are for stars with $T_{\rm eff} > 6200$ K, while blue points are for cooler stars.

We call attention to two patterns: (1) for hot stars, the chance of being significantly misaligned does not seem to depend on either of these two parameters; (2) for cool stars, the misaligned

[4] The data were collated with the help of *TEPCat* (Southworth 2011), René Heller's webpage, exoplanet.eu, and exoplanets.org. For those few systems with more than one planet, we used the properties of the most massive planet. We omitted 55 Cnc e, because although Bourrier & Hébrard (2014) reported a high obliquity, we are persuaded by the more precise data of López-Morales et al. (2014), which states that the obliquity is unknown.

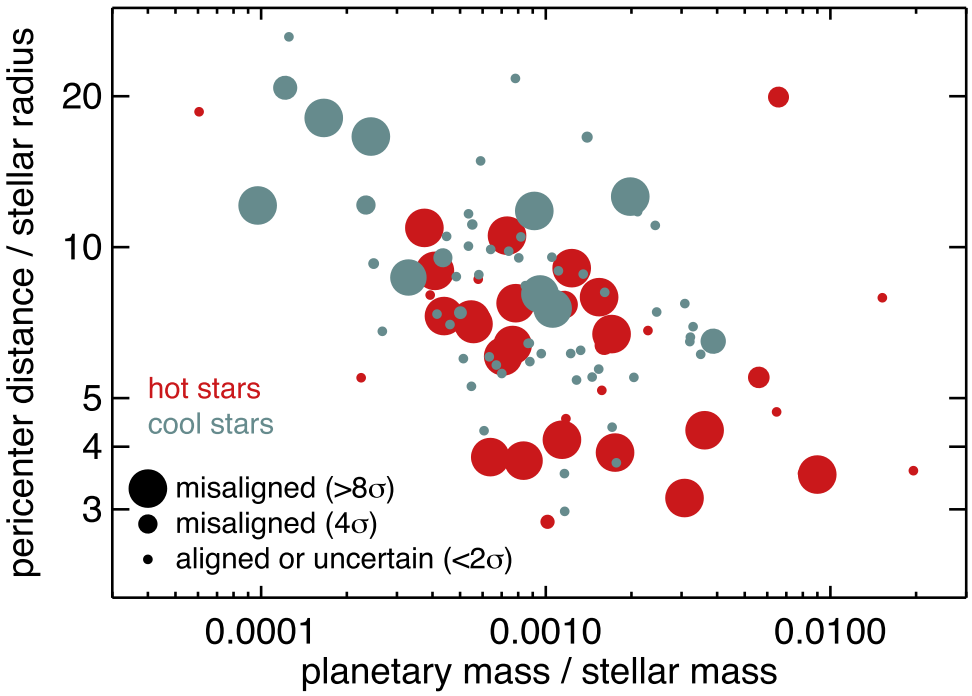

Figure 5. Measurements of stellar obliquity as a function of $M_p/M_\star$, the planet-to-star mass ratio, and $a_{\rm min}/R_\star$, the pericenter distance in units of the stellar radius. Red points are for stars with $T_{\rm eff} > 6200$ K (generally $>1.2\ M_\odot$) and blue points are for cooler stars. The symbol size increases with $n_\sigma \equiv |\lambda|/\sigma_\lambda$, the confidence with which a nonzero obliquity can be excluded. The smallest symbols have $n_\sigma < 2$, the largest symbols have $n_\sigma > 8$, and in between the symbol size is proportional to n_σ.

stars are all in the zone $a_{\rm min}/R_\star \gtrsim 8$. Similar patterns were noted earlier by Winn et al. (2010a), who speculated that the key physical mechanism distinguishing these cases is tidal realignment. In this picture, more rapid realignment is possible for cool stars, because of more rapid dissipation associated with their thick convective envelopes; and it is also more rapid for massive close-in planets, because of the stronger tides they raise. Indeed, Albrecht et al. (2012) showed that for cool stars, the boundary between aligned and misaligned stars could be expressed as a threshold value of $(M_p/M_\star)^2(a/R_\star)^{-5}$, a parameter that should be proportional to tidal dissipation rate in the theory of Zahn (1977). Through modeling of the structure of each star, Valsecchi & Rasio (2014) even found evidence that the aligned stars tend to have thicker convective zones.

However, tidal realignment theories suffer from a theoretical problem: they need to avoid concomitant orbital decay (Winn et al. 2010a; Dawson 2014). This problem might be superable (Lai 2012; Li & Winn 2016), but another problem emerged recently from a study by Mazeh et al. (2015b). They found statistical evidence for the hot/cool obliquity distinction even in cases where tidal interactions should be utterly negligible, i.e., low-mass planets in wide orbits. We also see from Figure 5 that while high $a_{\rm min}/R_\star$ is associated with misalignment, there is no evidence for any separate dependence on $M_p/M_\star$, even though this parameter should also be important in determining tidal effects. For these reasons, scenarios involving tidal realignment are questionable.

Many scenarios have been presented to try and explain the high obliquities of some planet-hosting stars. Any successful theory must explain why the obliquity distributions are different for hot and cool stars. Judging from Figure 5, a successful theory should probably also distinguish between wide- and close-orbiting planets around cool stars.

Mechanisms that simply tilt the protoplanetary disk at an early stage, such as the chaotic accretion of Bate et al. (2010) or the stellar flybys of Batygin (2012), do not have these properties. Neither do theories involving planet scattering or the Kozai effect (see, e.g., Fabrycky & Tremaine 2007; Chatterjee et al. 2008). These theories could be combined with a tidal realignment mechanism to produce the hot/cool distinction, but as we have already said, this solution is problematic. Rogers et al. (2012) proposed a mechanism to tilt hot stars, but were silent about the cool stars with high obliquities. Matsakos & Königl (2015) and Spalding & Batygin (2015) presented two ways to avoid the theoretical problem with tidal realignment. The former authors propose the host stars were realigned by ingesting a hot Jupiter that is no longer observable, while the latter authors, following Lai et al. (2011), invoke magnetic interactions with the inner edge of the protoplanetary disk. However, they do not discuss why these processes should depend on the $a_{\rm min}/R_\star$ of the innermost surviving giant planet. In short, we are not aware of any single proposed mechanism that can explain all of the obliquity data.

References

Albrecht, S., Winn, J. N., Johnson, J. A., et al. 2012, ApJ, 757, 18
Anderson, D. R., Collier Cameron, A., Delrez, L., et al. 2017, arXiv:1701.03776
Bakos, G. A., Torres, G., Pál, Á., et al. 2010, ApJ, 710, 1724
Barnes, J. W. 2009, ApJ, 705, 683
Bate, M. R., Lodato, G., & Pringle, J. E. 2010, MNRAS, 401, 1505
Batygin, K. 2012, Natur, 491, 418
Béky, B., Kipping, D. M., & Holman, M. J. 2014, MNRAS, 442, 3686
Borucki, W. J., Koch, D. G., Basri, G., et al. 2011, ApJ, 736, 19
Bourrier, V., & Hébrard, G. 2014, A&A, 569, A65
Chaplin, W. J., Sanchis-Ojeda, R., Campante, T. L., et al. 2013, ApJ, 766, 101
Chatterjee, S., Ford, E. B., Matsumura, S., & Rasio, F. A. 2008, ApJ, 686, 580
Dawson, R. I. 2014, ApJL, 790, L31

Deming, D., Knutson, H., Kammer, J., et al. 2015, ApJ, 805, 132
Désert, J.-M., Charbonneau, D., Demory, B.-O., et al. 2011, ApJS, 197, 14
Fabrycky, D., & Tremaine, S. 2007, ApJ, 669, 1298
Foreman-Mackey, D., Hogg, D. W., Lang, D., & Goodman, J. 2013, PASP, 125, 306
Howell, S. B., Sobeck, C., Haas, M., et al. 2014, PASP, 126, 398
Kreidberg, L. 2015, PASP, 127, 1161
Lai, D. 2012, MNRAS, 423, 486
Lai, D., Foucart, F., & Lin, D. N. C. 2011, MNRAS, 412, 2790
Li, G., & Winn, J. N. 2016, ApJ, 818, 5
Lomb, N. R. 1976, Ap&SS, 39, 447
López-Morales, M., Triaud, A. H. M. J., Rodler, F., et al. 2014, ApJL, 792, L31
Masuda, K. 2015, ApJ, 805, 28
Matsakos, T., & Königl, A. 2015, ApJL, 809, L20
Mazeh, T., Holczer, T., & Shporer, A. 2015a, ApJ, 800, 142
Mazeh, T., Perets, H. B., McQuillan, A., & Goldstein, E. S. 2015b, ApJ, 801, 3
McQuillan, A., Aigrain, S., & Mazeh, T. 2013, MNRAS, 432, 1203
Newville, M., Stensitzki, T., Allen, D. B., & Ingargiola, A. 2014, LMFIT: Non-Linear Least-Square Minimization and Curve-Fitting for Pythonű, Zenodo, doi:10.5281/zenodo.11813
Nutzman, P. A., Fabrycky, D. C., & Fortney, J. J. 2011, ApJL, 740, L10
Queloz, D., Mayor, M., Weber, L., et al. 2000, A&A, 354, 99
Rogers, T. M., Lin, D. N. C., & Lau, H. H. B. 2012, ApJL, 758, L6
Sanchis-Ojeda, R., & Winn, J. N. 2011, ApJ, 743, 61
Sanchis-Ojeda, R., Winn, J. N., Holman, M. J., et al. 2011, ApJ, 733, 127
Scargle, J. D. 1982, ApJ, 263, 835
Schlaufman, K. C. 2010, ApJ, 719, 602
Southworth, J. 2011, MNRAS, 417, 2166
Spalding, C., & Batygin, K. 2015, ApJ, 811, 82
Valsecchi, F., & Rasio, F. A. 2014, ApJ, 786, 102
Vanderburg, A., & Johnson, J. A. 2014, PASP, 126, 948
Winn, J. N., Fabrycky, D., Albrecht, S., & Johnson, J. A. 2010a, ApJL, 718, L145
Winn, J. N., & Fabrycky, D. C. 2015, ARA&A, 53, 409
Winn, J. N., Johnson, J. A., Howard, A. W., et al. 2010b, ApJL, 723, L223
Zahn, J.-P. 1977, A&A, 57, 383